A comparative study of the endocasts of OH 5 and SK 1585: Implications for the paleoneurology of eastern and southern African *Paranthropus*

Amélie Beaudet[a,b,c*], Ralph Holloway[d], Stefano Benazzi[e,f]

[a] *Department of Archaeology, University of Cambridge, Cambridge, United Kingdom*
[b] *School of Geography, Archaeology and Environmental Studies, University of the Witwatersrand, Johannesburg, South Africa*
[c] *Institut Català de Paleontologia Miquel Crusafont, Universitat Auto` noma de Barcelona, Barcelona, Spain*
[d] *Department of Anthropology, Columbia University, New York, USA*
[e] *Department of Cultural Heritage, University of Bologna, Ravenna, Italy*
[f] *Department of Human Evolution, Max Planck Institute for Evolutionary Anthropology, Leipzig, Germany*

***Corresponding author**
E-mail address: beaudet.amelie@gmail.com (A. Beaudet).

Acknowledgments

We are indebted to S. Potze and M. Tawane (Pretoria), L. Bam, F. de Beer and J. Hoffman (Pelindaba) for collection access and data acquisition. Model-based deformation computation was granted access to the supercomputing centre of CHPC (AB). For scientific contributions and/or discussion, the authors are especially grateful to J. Braga (Toulouse), J. Dumoncel (Toulouse), A. Oettlé (Pretoria), D. Stratford (Johannesburg) and J.F. Thackeray (Johannesburg). We thank the Editor, Associate Editor and three anonymous reviewers for their comments, which contributed to improving the original version of this manuscript. A.B. is funded by the DST-NRF Center of Excellence in Palaeosciences (CoE-Pal) and the University of the Witwatersrand. S.B. is funded by the European Research Council (ERC) under the European Union's Horizon 2020 research and innovation programme (grant agreement No 724046–SUCCESS, http://www.erc-success.eu). Opinions expressed and conclusions arrived at, are those of the author and are not necessarily to be attributed to the CoE-Pal.

Short Communications

A comparative study of the endocasts of OH 5 and SK 1585: Implications for the paleoneurology of eastern and southern African *Paranthropus*

Keywords: Brain shape; Early hominins; Olduvai Gorge; Swartkrans; Surface-based comparison

1. Introduction

The taxonomy, phylogeny and biology of the *Paranthropus* species have been the center of debates since the earliest discovery of the TM 1517 (now attributed to *Paranthropus robustus*) cranium from the Plio-Pleistocene site of Kromdraai (South Africa) in 1938 by R. Broom. In particular, whether *Paranthropus boisei* and *P. robustus* represent two distinct taxa, and whether the two species emerged from a common ancestor (i.e., hypothesis of a monophyletic group), remain largely unresolved (reviewed in Constantino and Wood, 2004, 2007; Wood and Schroer, 2017). Besides the taxonomic and phylogenetic aspects, the presence of two contemporaneous 'robust' species in the eastern and southern African hominin fossil records raises critical questions regarding potential occurrences of homoplasies in the hominin clade, with substantial implications for our understanding of early hominin paleobiology (Wood and Schroer, 2017). Moreover, the absence of associated cranial and postcranial remains attributed to *Paranthropus* complicate the reconstruction of the behaviour of this enigmatic 'megadont' hominin genus (reviewed in Constantino and Wood, 2007).

In this respect, brain endocasts may have the potential to provide additional insights into the taxonomy, phylogeny and behavior of *Paranthropus* taxa. Until now, only a few studies have attempted to assess the evolutionary polarity of the cerebral features in *Paranthropus*, and even fewer have addressed the question of potential similarities and differences in the brain of the two regional variants of *Paranthropus*. By investigating the endocasts of *Paranthropus aethiopicus*, *P. boisei* and *P. robustus*, Falk et al. (2000) suggested substantial similarities between *Paranthropus* and extant chimpanzees and gorillas (i.e., similar overall endocranial dimensions, beak-shaped profile frontal lobes, rounded temporal poles) and hypothesized a less derived cerebral condition in *Paranthropus* as compared to *Australopithecus*. However, the description of the sulcal pattern in *P. robustus* (SK 1585) revealed a configuration of the lunate sulcus that is more similar to extant humans than to extant chimpanzees, thus suggesting a possible reorganisation of the cortical pattern (Holloway, 1972). However, there is an ongoing debate as to whether the lunate sulcus is homologous between apes and humans (e.g., Allen et al., 2006; Malikovic et al., 2012) and on the position of the lunate sulcus in early hominins (e.g., Falk, 1980, 1983, 2009; Holloway, 1981; Holloway et al., 2004a; Falk et al., 2018; Gunz et al., 2020; but see Holloway et al., 2016). Interestingly, Holloway (1972) identified critical similarities in the overall shape of the endocast between *P. boisei* (OH 5) and *P. robustus* (SK 1585; see Figs. 6–8 in Holloway, 1972), notwithstanding differences in the cerebellum with a rounded shape in *P. boisei* (Omo L338y-6) and a triangular shape for *P. robustus* (SK 1585; Holloway, 1972, 1981).

Given the ongoing debate on the evolutionary polarity of the *Paranthropus* cerebral features, in this paper we (i) test the hypothesis of a nonhuman, ape-like endocast in *Paranthropus* and a less derived condition as compared to *Australopithecus* (Falk et al., 2000), and (ii) investigate further potential morphological similarities between the eastern and southern *Paranthropus* endocasts (Holloway, 1972). Morphological affinities are quantitatively assessed through the application of a deformation-based method (Durrleman et al., 2012; Beaudet et al., 2016, 2018). Because of their remarkable degree of preservation, we focus our study on the endocasts of OH 5 (*P. boisei*) and SK 1585 (*P. robustus*). More specifically, we compare OH 5 and SK 1585 to extant humans, common chimpanzees (*Pan troglodytes*) and bonobos (*Pan paniscus*) and to the *Australopithecus* specimen Sts 5, using statistical shape analyses and color maps that render global and local morphological differences and similarities between groups/specimens.

2. Materials and methods

2.1. Samples

The two *Paranthropus* specimens included in our study, i.e., OH 5 and SK 1585, represent the most complete and well-preserved evidence currently available in the fossil record of the *P. boisei* and *P. robustus* endocasts, respectively (Holloway, 1972; Benazzi et al., 2011). The OH 5 face and neurocranium were found in 1959 by Leakey (1959) from the Bed I of Olduvai Gorge and dated to 1.85 Ma. This specimen was first published as the holotype of the hominin species *Zinjanthropus boisei*, which is now included in the genus *Paranthropus* (Tamrat et al., 1995). The face and neurocranium of OH 5 were scanned by computed tomography (CT) at the Radiologie 2 Department at Medizinische Universität Innsbruck (Austria) with a resolution of 0.48 x 0.48 x 1 mm. Benazzi et al. (2011) virtually reconstructed the OH 5 cranium by combining semilandmark-based geometric morphometric methods and computer-aided design techniques and using KNM-ER 406 as a reference, and produced a complete endocast (Fig. 1).

SK 1585 represents a natural endocast of *P. robustus* from the lime miners' rubble dump at Swartkrans (Brain, 1970). Although the stratigraphic provenance is not clear, the maximum age is estimated to about 2.19 Ma, based on the cosmogenic nuclide burial dating of Member 1 (Gibbon et al., 2014). The endocast preserves the right hemisphere and a very small portion of the left occipital lobe (Holloway, 1972; Fig. 1). SK 1585 was scanned at the South African Nuclear Energy Corporation in Pelindaba (South Africa) at a resolution of 0.066 mm (Fig. 1; Beaudet et al., 2019). We generated a virtual surface of the natural endocast of SK 1585 using Avizo v. 9.0 (Visualization Sciences Group Inc., Berlin). For comparative purposes,

we included the nearly complete endocast of the *Australopithecus africanus* specimen Sts 5 from the Sterkfontein Caves in South Africa (Broom, 1947; for further details see Beaudet et al., 2018).

In terms of extant comparative material, we included 10 *Homo sapiens*, 10 *Pan troglodytes* and 10 *Pan paniscus* with equal proportion of fully mature males and females. The sample of *Homo* was obtained from the human clinical records of the Pasteur Hospital in Toulouse, France, while the *Pan* samples were obtained from the Royal Museum for Central Africa, Tervuren, Belgium (Beaudet et al., 2018). The human and nonhuman specimens were scanned by medical CT with a resolution of 0.49–0.50 and 0.39–0.80, mm respectively.

2.2. Methods of analysis

To investigate the nature of the morphological differences between the fossil specimens and the extant groups, we used a size-independent and landmark-free registration method based on smooth and invertible surface deformation by using the software Deformetrica v4 (Durrleman et al., 2012; Beaudet et al., 2018). In this paper, we follow the method detailed in Beaudet et al. (2018). First, the surfaces were automatically aligned in position, orientation, and scale using one surface randomly selected as a reference. This was performed by using the tool "Align surfaces" available in Avizo v. 9.0 which is based on the iterative closest point algorithm that minimizes the root mean square distance between the points of each specimen to corresponding points on the reference (Besl and McKay, 1992). The option "rigid + uniform scale" was selected to remove the siz . A template was deformed to each extant specimen. From this process, a global mean shape was generated (Durrleman, 2010). Based on the deformation fields from the global mean shape to each extant specimen, we computed taxon-specific mean shapes (i.e., *Homo sapiens*, *Pan troglodytes* and *Pan paniscus*; Fig. 1). Then, the global mean shape, as well as the taxon-specific mean shapes, were deformed to the fossil specimens. The global mean shape and the deformation fields represent an atlas (Durrleman et al., 2012). In addition, we deformed the endocast of Sts 5 to the endocast of OH 5. In this analysis, we used a total of 22,275 control points with a kernel width parameter of 5.

We ran a second analysis using only the preserved endocranial region in SK 1585 following the method detailed in Dumoncel et al. (2016; see also Fig. 1 in Beaudet et al., 2018). Accordingly, the region corresponding to the missing surface in SK 1585 was virtually removed from each endocast included in our sample and we computed a second atlas as well as global and taxon-specific mean shapes that were deformed to the fossil endocasts (Beaudet

et al., 2018). Finally, we deformed Sts 5 to SK 1585, and SK 1585 to OH 5. In this analysis, we used a total 17 600 control points with a kernel width parameter of 5.

The 3D deformation fields integrating local orientation and the amplitude of the two deformation sets were statistically analyzed by principal component analyses (PCA) using complete (i.e., extant *Homo* and *Pan* specimens, OH 5 and Sts 5) and partial (i.e., extant *Homo* and *Pan* specimens, OH 5, SK 1585 and Sts 5) endocasts to quantify shape variation. Signs were obtained by comparing the displacements of the direction perpendicular to the tangential surface, and those signs were applied to the magnitude and orientation of the displacements recorded during the deformation process. Signed distances are rendered by color maps from dark blue, indicating negative values and, thus, flatter surfaces, to red, indicating positive values, and thus more bulging surfaces (Beaudet and Bruner, 2017). In this respect, similar colors indicate similar amount and orientation of displacements between the fossil specimens and the mean shapes, or between fossil specimens. The codes (developed with Python and R) used for the post-processing steps (i.e., PCA, signed color maps) are available at https://gitlab.com/jeandumoncel/tools-for-deformetrica (Beaudet et al., 2018).

3. Results

The general shapes of the endocasts of the *Paranthropus* specimens OH 5 and SK 1585 are visually compared with the *Australopithecus* specimen Sts 5 and with the extant human, common chimpanzee and bonobo taxon-specific mean shapes in Figure 1. Results of the deformation process are shown in Figure 2 (statistical analyses) and Figures 3–4 (color maps).

The statistical analysis of shape variation using scaled complete endocasts (Fig. 2A) indicates that the morphology of the endocast of OH 5 closely approximates the morphology of *Pan* (and more particularly *P. paniscus*) along PC1. By contrast, Sts 5 falls in between the *Homo* and *Pan* clusters. The statistical analysis of the scaled partial endocast (Fig. 2B) shows that the morphology of the endocasts of the two *Paranthropus* specimens OH 5 and SK 1585 are more similar to *Pan* than to *Homo* along both axes, while Sts 5 plots in between *Homo* and *Pan* along PC1, as in the previous analysis.

The dorsal surface of the parietal lobes in OH 5 and SK 1585 is more flattened dorsoventrally than in *Homo* and more bulging than in *Pan* (Fig. 3). Moreover, the dorsal surface of the frontal lobes in both fossil specimens is more flattened dorsoventrally than in *Homo* and *Pan* except along the superior sagittal sinus. The temporoparietal and temporooccipital areas in OH 5 and SK 1585, that encompass the inferior parietal lobule where the supramarginal and angular gyri are located, are more pronounced than in *Homo* but less

than in *Pan*. Moreover, the inferior frontal gyrus is less developed in OH 5 and in SK 1585 than in *Homo*, but slightly more developed than in *Pan* in the case of SK 1585. The cerebellar lobes in the fossil specimens and in *Pan* protrude more laterally than in *Homo*.

The endocasts of the *Paranthropus* specimens OH 5 and SK 1585 differ from the endocast of the *Australopithecus* specimen Sts 5 by displaying more flattened frontal lobes dorsoventrally, temporal lobes and parietooccipital regions that are more laterally expanded, and less protruding cerebellar lobes (Fig. 4). The areas that mainly differ between OH 5 and SK 1585 correspond to cracks visible on the right parietal and temporal regions of the endocast of OH 5 (Figs. 1 and 4).

4. Discussion

Overall, within the limits of our sample, the two *Paranthropus* specimens share with the extant common chimpanzees and bonobos a laterally broad and dorsoventrally flattened endocast (Figs. 1 and 3), a morphology that has been previously described in *Australopithecus* through the use of the deformation-based method. However, our statistical analyses and color maps indicate that the *A. africanus* specimen Sts 5 is intermediate between the extant human and chimpanzee conditions and less laterally narrower and less dorsoventrally flattened than in the *Paranthropus* specimens (Fig. 2). Even if limited by one specimen per species, our study of shape variation provides additional support for the affinities of the shape of the *Paranthropus* endocast with nonhuman apes and the hypothesis of a less derived endocast in *Paranthropus* as compared to *Australopithecus* (Falk et al., 2000). If we consider the hypothesis of a brain shape in early *Homo* that is more modern human-like than ape-like (e.g., Tobias, 1991), our results may suggest distinct brain evolutionary histories between the contemporaneous hominin genera *Homo* and *Paranthropus*. Moreover, the human-like configuration of the lunate sulcus in *Paranthropus*, as revealed by Holloway (1972), raises questions of the timing and pattern of the evolution of the brain, and may imply that cortical reorganization occurred without noticeable changes in overall shape of the brain. Investigating a larger sample using this deformation-based approach would be of particular interest to evaluate patterns of intraspecific variation and further address these questions (Neubauer et al., 2012).

The frontal lobes are of particular interest because of their role in executive functions and language (e.g., Kringelbach and Rolls, 2004; Petrides and Pandya, 1999; Rajkowska and Goldman-Rakic, 1995; Schenker et al., 2010). The frontal lobes in the *Paranthropus* specimens are relatively flattened as compared to *Homo* and *Pan*. Rather than reflecting potential cerebral

changes, this morphological specificity could be related to masticatory hypertrophy and structural constraints imposed by the integration of the face with the braincase (Wu and Bruner, 2016; Beaudet and Bruner, 2017). Our study indicates substantial morphological differences in the area that encompasses the inferior temporal lobule, including the supramarginal and angular gyri, between the two *Paranthropus* specimens and *Homo* (i.e., more pronounced in *Paranthropus*), and between the two *Paranthropus* specimens and *Pan* (i.e., less pronounced in *Paranthropus*). Since this region is part of the somatosensory association cortex (Mountcastle et al., 1974; Celsis et al., 1999; Seghier, 2013), differences in this area between *Paranthropus, Homo* and *Pan* might have potential behavioral implications (e.g., locomotion, manipulation). However, these interpretations would need to be further explored in the future by the comparative study of the sulcal pattern in these key cerebral regions in the endocasts of these taxa. The cerebellar lobes of the two *Paranthropus* specimens protrude more laterally than in extant humans but less than in Sts 5, which confirms previous observations (Holloway, 1972). As for the supramarginal and angular gyri, differences between the *Paranthropus*, *Australopithecus* and extant specimens might be interpreted as potential evidence suggesting distinct behaviours because of the role of these regions in fundamental motor-related functions (e.g., Kochiyama et al., 2018; Neubauer et al., 2018).

Finally, the overall shapes of the endocasts of the *P. boisei* specimen OH 5 and the *P. robustus* specimen SK 1585 are relatively similar (Fig. 4), as previously pointed out by Holloway (1972). Similarities between eastern and southern African *Paranthropus* would need to be confirmed by future studies of more complete endocasts of southern African *Paranthropus*.

References

Allen, J. S., Bruss, J., Damasio, H., 2006. Looking for the lunate sulcus: A magnetic resonance imaging study in modern humans. Anat. Rec. 288, 867–876.

Beaudet, A., Bruner, E., 2017. A frontal lobe surface analysis in three archaic African human fossils: OH 9, Buia, and Bodo. C. R. Palevol. 16, 499–507.

Beaudet, A., Dumoncel, J., de Beer, F., Duployer, B., Durrleman, S., Gilissen, E., Hoffman, J., Tenailleau, C., Thackeray, J.F., Braga, J., 2016. Morphoarchitectural variation in South African fossil cercopithecoid endocasts. J. Hum. Evol. 101, 65–78.

Beaudet, A., Dumoncel, J., de Beer, F., Durrleman, S., Gilissen, E., Oettle, A., Subsol, G., Thackeray, J.F., Braga, J., 2018. The endocranial shape of *Australopithecus africanus*: Surface analysis of the endocasts of Sts 5 and Sts 60. J. Anat. 232, 296–303.

Beaudet, A., Clarke, R.J., de Jager, E., Bruxelles, L., Carlson, K.J., Crompton, R., de Beer, F., Dhaene, J., Heaton, J.L., Jakata, K., Jashashvili, T., Kuman, K., McClymont, J., Pickering, T.R., Stratford, D., 2019. The endocast of StW 573 ("Little Foot") and hominin brain evolution. J. Hum. Evol. 126, 112–123.

Benazzi, S., Bookstein, F.L., Strait, D., Weber, G.W., 2011. A new OH5 reconstruction with an assessment of its uncertainty. J. Hum. Evol. 61, 75–88.

Besl, P.J., McKay, N.D., 1992. A method for registration of 3-D shapes. IEE Trans. Pattern Anal. 14, 239–256.

Brain, C.K., 1970. New finds at the Swartkrans australopithecine site. Nature 225, 1112–1119.

Broom, R., 1938. The Pleistocene anthropoid apes of South Africa. Nature 142, 377–379.

Broom, R., 1947. Discovery of a new skull of the South African ape-man, *Plesianthropus*. Nature 159, 672.

Celsis, P., Boulanouar, K., Doyon, B., Ranjeva, J.P., Berry, I., Nespoulous, J.L., Chollet, F., 1999. Differential fMRI responses in the left posterior superior temporal gyrus and left supramarginal gyrus to habituation and change detection in syllables and tones. Neuroimage 9, 135–144.

Constantino P, Wood B. 2004. *Paranthropus paleobiology*. Miscelánea en homenaje a Emiliano Aguirre. Museo Arqueolócico Regional, Madrid, pp. 136–151.

Constantino, P., Wood, B., 2007. The evolution of *Zinjanthropus boisei*. Evol. Anthropol. 16, 49–62.

Dumoncel, J., Subsol, G., Durrleman, S., Jessel, J.-P., Beaudet, A., Braga, J., 2016. How to build an average model when samples are variably incomplete? Application to fossil data. Proceedings of the IEEE Conference on Computer Vision and Pattern Recognition (CVPR) Workshops, pp. 541-548.

Durrleman, S., 2010. Statistical models of currents for measuring the variability of anatomical curves, surfaces and their evolution. Ph.D. Dissertation, Université Nice-Sophia Antipolis.

Durrleman, S., Pennec, X., Trouvé, A., Ayache, N., Braga, J., 2012. Comparison of the endocranial ontogenies between chimpanzees and bonobos via temporal regression and spatiotemporal registration. J. Hum. Evol. 62, 74–88.

279 Falk, D., 1980. A reanalysis of the South African australopithecine natural endocasts. Am. J.
280 Phys. Anthropol. 53, 525–539.
281 Falk, D., 1983. Cerebral cortices of East African early hominids. Science 221, 1072–1074.
282 Falk, D., 2009. The natural endocast of Taung (*Australopithecus africanus*): Insights from the
283 unpublished papers of Raymond Arthur Dart. Am. J. Phys. Anthropol. 49, 49-65.
284 Falk, D., Redmond Jr., J.C., Guyer, J., Conroy, G.C., Recheis, W., Weber, G.W., Seidler, H.,
285 2000. Early hominid brain evolution: A new look at old endocasts. J. Hum. Evol. 38,
286 695–717.
287 Falk, D., Zollikofer, C.P.E., Ponce de León, M., Semendeferi, K., Alatorre Warren, J.L.,
288 Hopkins, W.D., 2018. Identification of in vivo sulci on the external surface of eight
289 adult chimpanzee brains: Implications for interpreting early hominin endocasts. Brain
290 Behav. Evol. 91, 45–58.
291 Gibbon, R.J., Pickering, T.R., Sutton, M.B., Heaton, J.L., Kuman, K., Clarke, R.J., Brain, C.K.,
292 Granger, D.E., 2014. Cosmogenic nuclide burial dating of hominin bearing Pleistocene
293 cave deposits at Swartkrans, South Africa. Quat. Geochronol. 24, 10–15.
294 Gunz, P., Neubauer, S., Falk, D., Tafforeau, P., Le Cabec, A., Smith, T.M., Kimbel, W.H.,
295 Spoor, F., Alemseged, Z., 2020. *Australopithecus afarensis* endocasts suggest ape-like
296 brain organization and prolonged brain growth. Sci. Adv. 6, eaaz4729.
297 Holloway, R.L., 1972. New australopithecine endocast, SK 1585, from Swartkrans, South
298 Africa. Am. J. Phys. Anthropol. 37, 173–186.
299 Holloway, R., 1981. The endocast of the Omo L338y-6 juvenile hominid: Gracile or robust
300 *Australopithecus*? Am. J. Phys. Anthropol. 54, 109–118.
301 Holloway, R.L., Clarke, R.J., Tobias, P.V., 2004a. Posterior lunate sulcus in *Australopithecus*
302 *africanus*: Was Dart right? C. R. Palevol. 3, 287–293.
303 Holloway, R.L., Broadfield, D.C., Yuan, M.S., 2004b. The Human Fossil Record: Brain
304 Endocasts, the Paleoneurological Evidence. Wiley-Liss, Hoboken.
305 Holloway, R.L., Schoenemann, P.T., Broadfield, D.C., 2016. Why paleoneurology needs the
306 lunate sulcus. Am. J. Phys. Anthropol. Suppl. 159, 175.
307 Kochiyama, T., Ogihara, N., Tanabe, H.C., Kondo, O., Amano, H., Hasegawa, K., Suzuki, H.,
308 Ponce de León, M.S., Zollikofer, C.P.E., Bastir, M., Stringer, C., Sadato, N., Akazawa,
309 T., 2018. Reconstructing the Neanderthal brain using computational anatomy. Sci. Rep.
310 8, 6296.

311 Kringelbach, M.L., Rolls, E.T., 2004. The functional neuroanatomy of the human orbitofrontal
312 cortex: evidence from neuroimaging and neuropsychology. Prog. Neurobiol. 72, 341–
313 372.
314 Leakey, L.S.B., 1959. A new fossil skull from Olduvai. Nature 201, 967–970.
315 Malikovic, A., Vucetic, B., Milisavljevic, M., Tosevski, J., Sazdanovic, P., Milojevic, B.,
316 Malobabic, S., 2012. Occipital sulci of the human brain: Variability and morphometry.
317 Anat. Sci. Int. 87, 61–70.
318 Mountcastle, V.B., Lynch, J.C., Georgopoulos, A., Sakata, H., Acuna, C., 1975. Posterior
319 parietal association cortex of the monkey: Command functions for operations within
320 extrapersonal space. J. Neurophysiol. 38, 871–908.
321 Neubauer, S., Gunz, P., Weber, G.W., Hublin, J.-J., 2012. Endocranial volume of
322 *Australopithecus africanus*: New CT-based estimates and the effects of missing data
323 and small sample size. J. Hum. Evol. 62, 498-510.
324 Neubauer, S., Hublin, J.-J., Gunz, P., 2018. The evolution of modern human brain shape. Sci.
325 Adv. 4, eaao5961.
326 Petrides, M., Pandya, D.N., 1999. Dorsolateral prefrontal cortex: Comparative
327 cytoarchitectonic analysis in the human and the macaque brain and corticocortical
328 connection patterns. Eur. J. Neurosci. 11, 1011–1036
329 Rajkowska, G., Goldman-Rakic, P.S., 1995. Cytoarchitectonic definition of prefrontal areas in
330 the normal human cortex: II. Variability in locations of areas 9 and 46 and relationship
331 to the Talairach Coordinate System. Cereb. Cortex 5, 323–337
332 Schenker, N.M., Hopkins, W.D., Spocter, M.A., Garrison, A.R., Stimpson, C.D., Erwin, J.M.,
333 Hof, P.R., Sherwood, C.C., 2010. Broca's area homologue in chimpanzees (*Pan*
334 *troglodytes*): Probabilistic mapping, asymmetry, and comparison to humans. Cereb.
335 Cortex 20, 730–742.
336 Seghier, M.L., 2013. The angular gyrus: Multiple functions and multiple subdivisions.
337 Neuroscientist 19, 43–61.
338 Tamrat, E., Thouveny, N., Taieb, M., Opdyke, N.D., 1995. Revised magnetostratigraphy of the
339 Plio-Pleistocene sedimentary sequence of the Olduvai formation (Tanzania).
340 Palaeogeogr. Palaeoclimatol. Palaeoecol. 114, 273–283.
341 Tobias, P.V., 1991. Olduvai Gorge. In: The Skulls, Endocasts and Teeth of *Homo habilis*, Vol.
342 4. Cambridge University Press, Cambridge.
343 Wood, B., Schroer, K., 2017. *Paranthropus*: Where do things stand? In: Marom, A., Hovers,
344 E. (Eds.), Human Paleontology and Prehistory. Springer, New York, pp. 95–107.

345 Wu, X., Bruner, E., 2016. The endocranial anatomy of Maba 1. Am. J. Phys. Anthropol. 160,
346 633–643.

Figure legends

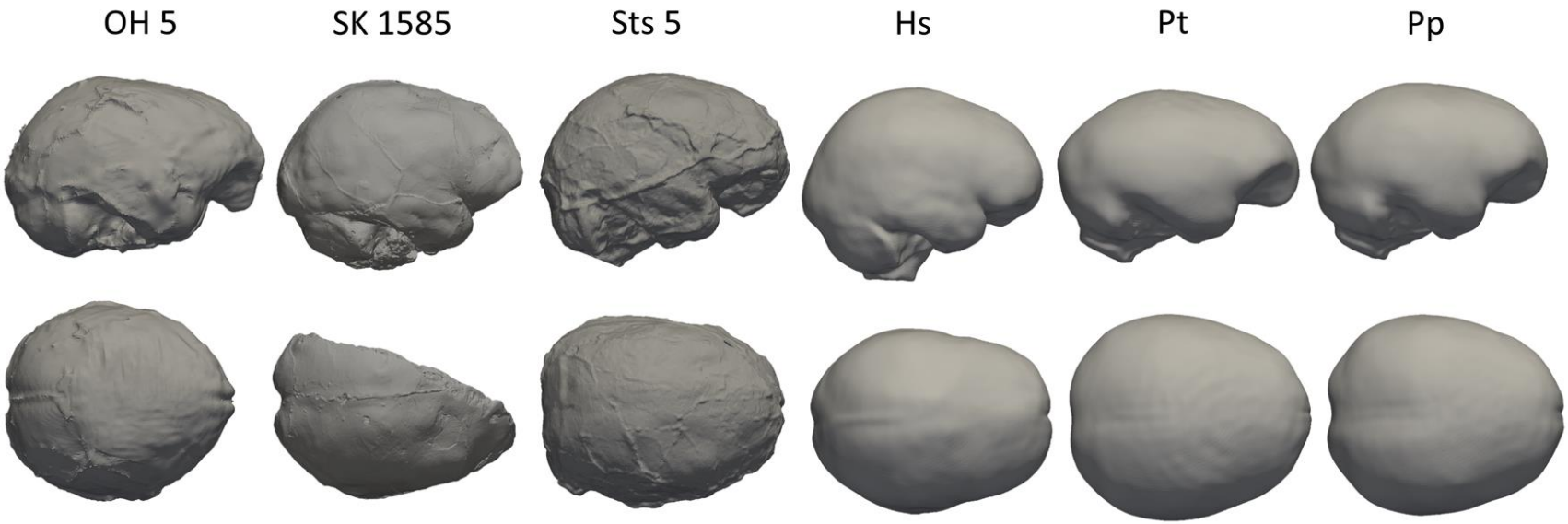

Figure 1. Virtual rendering of the endocasts of the *Paranthropus* specimens OH 5 (*P. boisei*) and SK 1585 (*P. robustus*) and Sts 5 (*Australopithecus africanus*), and the taxon-specific mean shapes of extant humans (Hs), common chimpanzees (Pt) and bonobos (Pp) in lateral right (top) and superior (bottom) views. Images not to scale.

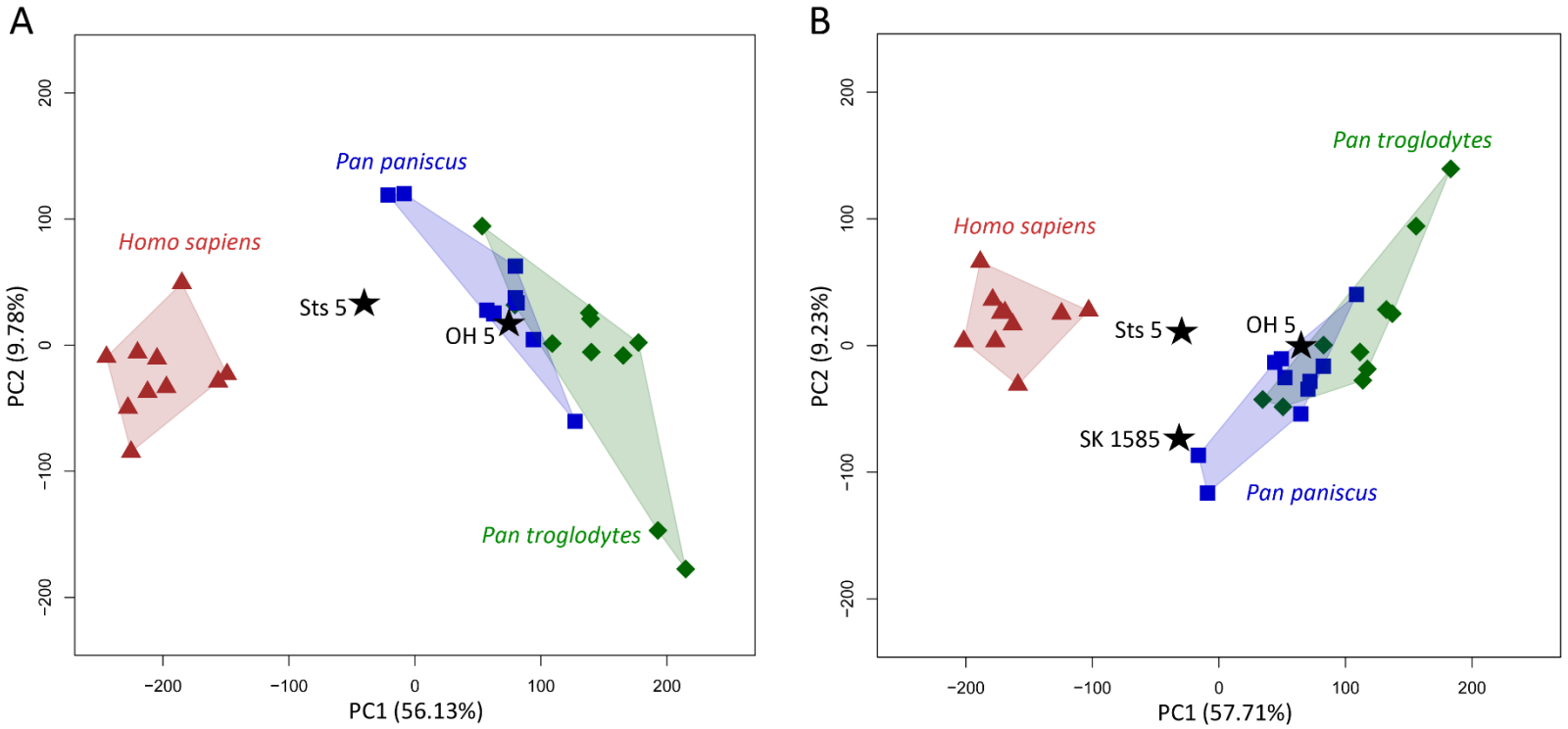

Figure 2. Principal component analyses of the deformation-based shape comparisons of the A) complete and B) partial *Paranthropus* (OH 5, SK 1585), *Australopithecus* (Sts 5), extant human (red triangles), common chimpanzee (green diamonds) and bonobo (blue squares) endocasts. OH 5 and SK 1585 are more similar to *Pan* than to *Homo* along both axes, while Sts 5 plots in between *Homo* and *Pan.*

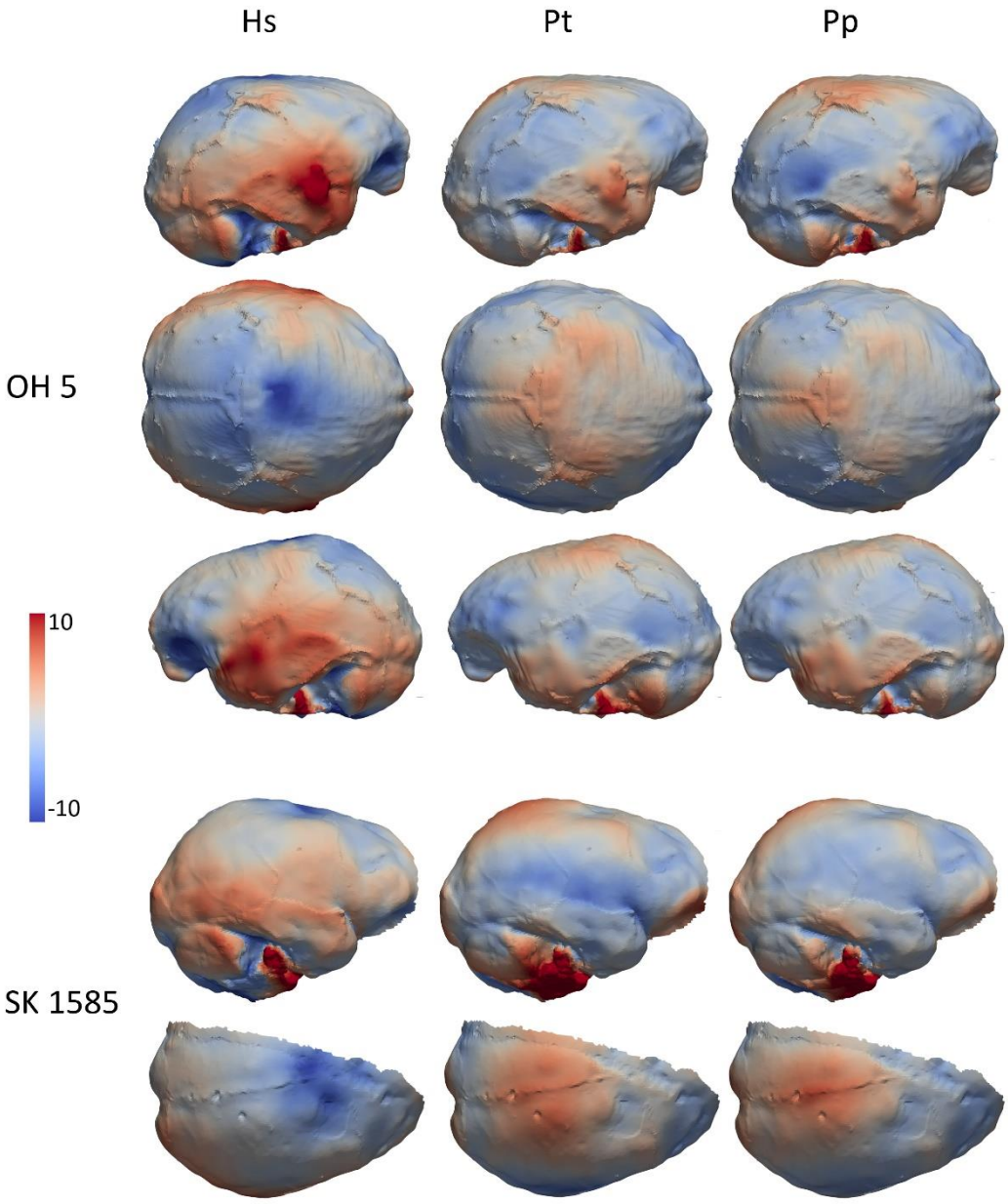

Figure 3. Comparative maps of morphological deformations from the extant human (Hs), common chimpanzee (Pt) and bonobo (Pp) mean shapes to the *Paranthropus* specimens OH 5 and SK 1585. Endocasts for OH5 are shown in lateral right (top row), superior (second row) and lateral left (third row) views. Endocasts for SK 1585 are shown in lateral right (fourth row) and superior (bottom row) views. Cumulative displacement variations (in mm) in the direction perpendicular to the tangential surface are rendered by a pseudocolor scale ranging from dark blue (highest negative values, more flatter surfaces) to red (highest positive values, more bulging surfaces) at the fossil surfaces.

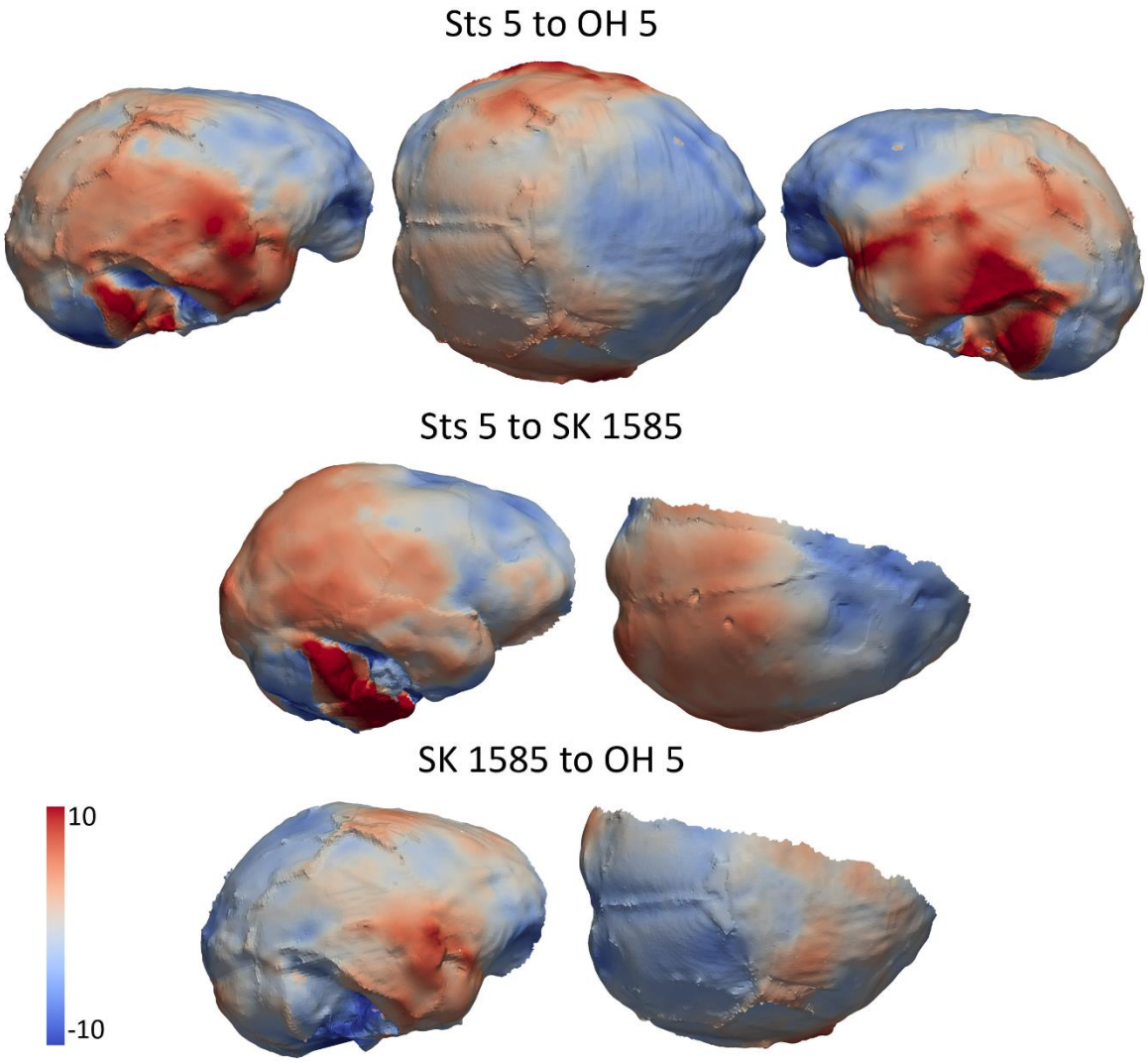

Figure 4. Comparative maps of morphological deformations from Sts 5 to OH 5 (top), from Sts 5 to SK 1585 (middle) and from SK 1585 to OH 5 (bottom). Endocasts are shown in lateral right, superior and lateral left (OH 5 only) views. Cumulative displacement variations (in mm) in the direction perpendicular to the tangential surface are rendered by a pseudocolor scale ranging from dark blue (highest negative values, more flatter surfaces) to red (highest positive values, more bulging surfaces) at the OH 5 (top and bottom) and SK 1585 (middle) surfaces.